




Vacancy-induced giant photogalvanic effect in TiSe₂ heterojunctions

Yuan Li ^{1,*}, Xinyu Cheng,¹ Ying Ding,¹ Longfei Guo,¹ Tianchen Wang,¹ Gaofeng Xu ^{1,†} and Wu-Ming Liu ^{2,‡}

¹Department of Physics, Hangzhou Dianzi University, Hangzhou, Zhejiang 310018, China

²Beijing National Laboratory for Condensed Matter Physics, Institute of Physics, Chinese Academy of Sciences, Beijing 100190, China



(Received 15 August 2023; revised 4 February 2024; accepted 27 March 2024; published 25 April 2024)

We adopt nonequilibrium Green's functions and density functional theory to study the effect of Se atom defects on the transport properties and the photocurrent of a 1*T*-TiSe₂ heterojunction. We calculate the photocurrent for two types of defect configurations under the excitation of the linearly polarized light. The results show that Se1 and Se2 vacancy defects can induce large photocurrents, which are explained in terms of the transmission spectrum. The photocurrent shows anisotropic behaviors for different illuminated directions. Meanwhile, the extinction ratio reflecting the polarization sensitivity can reach a maximum value of 445.12. The photoresponsivities of the device with vacancy defects can have relatively large values in certain energy ranges. The 1*T*-TiSe₂-based device is a promising candidate for anisotropic light detection.

DOI: [10.1103/PhysRevB.109.165438](https://doi.org/10.1103/PhysRevB.109.165438)

I. INTRODUCTION

After the discovery of graphene [1], two-dimensional (2D) materials have aroused considerable interest in recent years. The *MX*₂ layered transition metal dichalcogenides (TMDs, *M* = Mo, W, V, Nb, Ta, Ti, Zr, Hf, or Re, and *X* = Se, S, or Te) are a large family of solids with layered triangular metal lattices [2]. They have rich electronic and optic properties, such as a high carrier mobility [3–5], a low effective mass [6,7], a layer-dependent tunable band gap [8,9], a direct-to-indirect band-gap crossover [10–12], and a nonlinear optical effect [13–15].

Compared with 2*H* phase TMDs, the research on the electronic and optical properties of 1*T* phase TMDs is relatively sparse. As a member of the 1*T* phase TMD family, 1*T*-TiSe₂ has been extensively studied owing to its charge density wave (CDW) ordering [16,17], and superconducting properties [18–20]. It is also proved to be an excellent system for observing the low-temperature CDW state [21,22]. The Ti atoms bond with their adjacent six Se atoms, shaping a Ti-Se octahedron unit cell and composing the basic framework of 1*T*-TiSe₂. Ti⁴⁺ atoms are located at the center of the composite, sandwiched between atoms in the Se²⁻ layer, forming an interlayer space (0.601 nm) between the two layers [23], which has an octahedral crystal structure with van der Waals stacked layers. 1*T*-TiSe₂, with its small semiconducting band gap, is one of the most explored in the TMD family, and its monolayer structure can be prepared by mechanical peeling methods.

There are some studies on the broadband saturation absorption [24,25], and the ultrafast and large optical nonlinearity [26,27] of monolayer 1*T*-TiSe₂. Ultrafast lasers can

generate and manipulate topological phase transitions and spin polarization in topological materials [28,29]. The defect modulation of 1*T*-TiSe₂ has received increasing attention, such as defect-controlled magnetism [30], short-range CDW and band-gap modulation of defects in TiSe₂ [31], and the effect of line defects on the catalytic activity [32]. A TiSe₂ system with defects shows great potential applications. However, relatively little theoretical research has studied the effect of defects on the photogalvanic effect (PGE) [33,34] and transport properties in 1*T*-TiSe₂-based devices. PGE is the second nonlinear photoresponse to the polarized light, which depends on the light polarization [35,36]. This makes PGE an attractive mechanism for polarization sensitivity and self-powered photodetection [37]. Nonlinear optical effects, such as finite rectified currents, can be described in a unified fashion by using the Keldysh Green's function method combined with the Floquet formalism [38,39]. We try to understand the performance impact of vacancy defects so that one can reliably implement them into devices.

II. THEORETICAL MODEL

As shown in Fig. 1(a), the gray and yellow spheres represent Ti and Se atoms, respectively. The space group of 1*T*-TiSe₂ is *P* $\bar{3}m1$, and the lattice constants are *a* = 3.54 Å, *b* = 3.54 Å, *c* = 6.008 Å. The band structure is given in Fig. 1(b), and 1*T*-TiSe₂ has a band gap of about 0.06 eV near the high-symmetry point *A*, which agrees well with those reported in Ref. [40].

We design a 1*T*-TiSe₂-based device and choose Cu as electrodes, which matches well with the central material. The TiSe₂-based device has 60 atoms in the absence of a vacancy defect. We focus on the effect of a Se vacancy defect on PGE at zero bias in a 1*T*-TiSe₂ heterojunction under the excitation of linearly polarized light (see the blue wavy lines), as shown in Fig. 1(c). We consider ten Se vacancies including two possible defect configurations, namely the Se1 and Se2 vacancy

*liyuan@hdu.edu.cn

†xug@hdu.edu.cn

‡wmliu@iphy.ac.cn

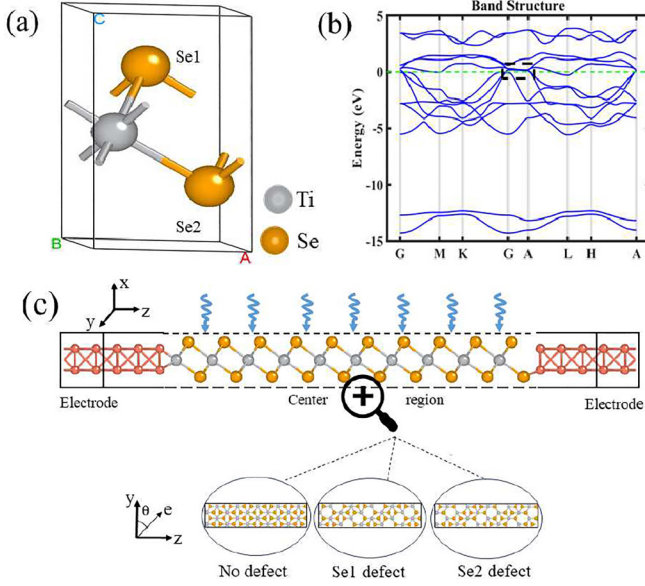


FIG. 1. (a) The unit cell structure of $1T$ -TiSe₂. (b) The band structure of $1T$ -TiSe₂. (c) Side view and top view of the heterojunction for different vacancy defects. Left: no defect; middle: Se1 vacancy defect; right: Se2 vacancy defect.

defects. The x , y , z axes are the vacuum, period, and transport directions, respectively.

The structure optimization and numerical calculations are performed by the quantum transport software NANODCAL [41]. The exchange-correlation potentials are treated by using the generalized gradient approximation (GGA) as parametrized by Perdew, Burke, and Ernzerhof [42]. The Brillouin zone of $1T$ -TiSe₂ is performed with an $18 \times 19 \times 1$ k mesh for geometry optimization and self-consistent calculations. The cutoff energy is set to 100 hartree (1 hartree = 27.21 eV). For the action of the linear polarized light, the electromagnetic potential is regarded as a weak interaction. The absorption processes are assumed to be dominated, thus neglecting the emission terms [43]. The photocurrent can be calculated by using the nonequilibrium Green's function (NEGF) method [43,44],

$$J_L^{(\text{ph})} = \frac{ie}{h} \int \left\{ \cos^2 \theta \text{Tr} \left\{ \Gamma_L [G_1^{<(\text{ph})} + f_L (G_1^{>(\text{ph})} - G_1^{<(\text{ph})})] \right\} \right. \\ \left. + \sin^2 \theta \text{Tr} \left\{ \Gamma_L [G_2^{<(\text{ph})} + f_L (G_2^{>(\text{ph})} - G_2^{<(\text{ph})})] \right\} \right. \\ \left. + \frac{\sin(2\theta)}{2} \text{Tr} \left\{ \Gamma_L [G_3^{<(\text{ph})} + f_L (G_3^{>(\text{ph})} - G_3^{<(\text{ph})})] \right\} \right\} dE, \quad (1)$$

where

$$G_1^{>/<(\text{ph})} = \sum_{\alpha, \beta=x,y,z} C_0 N G_0^R e_{1\alpha} p_\alpha^\dagger G_0^{>/<} e_{1\beta} p_\beta G_0^A, \\ G_2^{>/<(\text{ph})} = \sum_{\alpha, \beta=x,y,z} C_0 N G_0^R e_{2\alpha} p_\alpha^\dagger G_0^{>/<} e_{2\beta} p_\beta G_0^A, \\ G_3^{>/<(\text{ph})} = \sum_{\alpha, \beta=x,y,z} C_0 N G_0^R (e_{1\alpha} p_\alpha^\dagger G_0^{>/<} e_{2\beta} p_\beta \\ + e_{2\alpha} p_\alpha^\dagger G_0^{>/<} e_{1\beta} p_\beta) G_0^A. \quad (2)$$

Here, L indicates the left electrode, the linewidth function $\Gamma_L = i(\Sigma_L^R - \Sigma_L^A)$ is relative with the retarded/advanced self-energy $\Sigma_L^{R/A}$, which can be calculated by solving the surface Green's function of the leads [45]. $G^{>/<(\text{ph})}$ is the greater/lesser Green's function including electron-photon interactions, f_L is the Fermi-Dirac distribution function. $C_0 = e^2 \hbar \sqrt{\mu_r \epsilon_r} I_\omega / (2m^2 \omega \epsilon N c)$, ω is the photon frequency, m is the bare electron mass, $I_\omega = Nc / (V \sqrt{\mu_r \epsilon_r})$ is the photon flux, μ_r is the relative magnetic susceptibility, ϵ_r is the relative dielectric constant, and N is the number of photons. The polarization vector $\hat{e} = \cos \theta \hat{e}_1 + \sin \theta \hat{e}_2$, θ indicating the polarization angle. Note that the normalized photocurrent, i.e., the photoresponse function, is calculated in terms of $J = J_L^{(\text{ph})} / e I_\omega$, which has a dimension of the area a_0^2 /photon with a_0 being the Bohr radius. The detailed derivation is given in Appendix A.

III. NUMERICAL RESULTS AND DISCUSSION

The photocurrent of the Cu-TiSe₂-Cu heterojunction was calculated as a function of the polarization angle θ at photon energies of 0.3, 0.8, and 2.4 eV. Figures 2(a)–2(c) show the photocurrents for different Se vacancy defects. The maximum values occur near the angles $\theta = 90^\circ$. All of photocurrents present sinusoidal functions with the polarization angle [41,46], which is consistent with the PGE phenomenon theory [47].

Next, we analyze the effect of the vacancy defect on the maximum photocurrent J_{max} . Figure 3(a) shows the variation trends of J_{max} as a function of the photon energy for two types of defect configurations. The linearly polarized light propagates along the $-x$ axis. The right-hand side of the dotted line is the visible-light region, and the left-hand side is the infrared-light region. We can see that the Cu-TiSe₂-Cu heterojunction can obtain a large photocurrent even though there exists a vacancy defect, which verifies $1T$ -TiSe₂ possessing good photoelectric performance. In the absence of the vacancy defect, there are seven peaks in the photon energy range from 0.1 to 2.7 eV. For example, the maximum photocurrent J_{max} is about 9.031 at a photon energy 0.8 eV, 6.974 at 1.1 eV, and 8.473 at 2.7 eV. Similarly, for the Se1 vacancy defect, there are five peaks for J_{max} , which are 7.610 at 0.4 eV, 4.457 at 1.2 eV, 6.105 at 1.6 eV, 5.848 at 2.2 eV, and 4.126 at 2.6 eV. For the Se2 vacancy defect, there are three peaks for J_{max} , which are 6.392 at 1.8 eV, 7.856 at 2.1 eV, and 11.126 at 2.4 eV. The device with the Se2 vacancy defect has a large photocurrent with a value about 11.126 in the visible-light region. While the device with the Se1 vacancy defect can obtain a relatively large photocurrent in the far infrared region. This phenomenon shows that different defect configurations can be utilized to control the absorption of the visible light and the infrared light.

We further calculate the photocurrent for the linearly polarized light illuminated along the $-y$ axis, as shown in Fig. 3(b). With no defect, J_{max} can reach 10.136 at a photon energy of 2.6 eV in the purple visible-light region, which is significantly different from the photocurrent given in Fig. 3(a). Obviously, the photocurrent depends on the propagating direction of the light, which gives anisotropic behaviors. For the device with the Se1 vacancy defect, the largest photocurrent is about

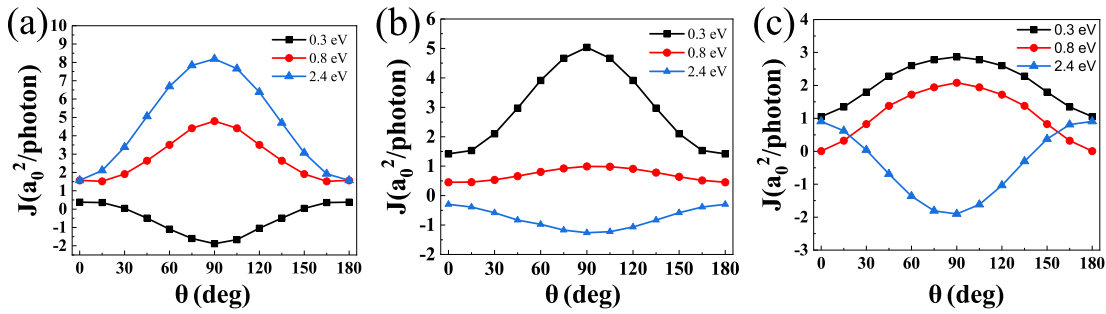


FIG. 2. The photocurrent is plotted as a function of the polarization angle θ for different photon energies for the defect configurations with (a) no defect, (b) Se1 vacancy defect, and (c) Se2 vacancy defect. The linearly polarized light propagates along the $-x$ axis.

7.670 at 0.4 eV. In this case, the device is more sensitive to the far infrared light. The photocurrent of the device with the Se2 vacancy defect has relatively smaller values than those of the former two defect configurations. There are two peaks with the photocurrent being 3.478 at 1.8 eV, and 4.071 at 2.5 eV. This phenomenon shows that the photocurrent can

be modulated by changing the defect configuration and the propagating direction of the light. We further calculate the transmission spectrum of the device to provide an intuitive understanding of the vacancy-induced photocurrent peaks. Figure 4 shows the variation trends of the transmission of the TiSe_2 -based device under the influence of the vacancy defect for the linearly polarized light propagating along the $-x$ axis. In the absence of the vacancy defect, as shown in Fig. 4(a), there are several transmission peaks, which mean that more quantum states contribute to the transmission at the Fermi energy. For example, two transmission peaks occur at -0.7 and 0.1 eV, thus it is possible for electrons jumping from the quantum state at -0.7 eV to the state at 0.1 eV. The electron's transition associates with the large photocurrent at the photon energy of 0.8 eV [see Fig. 3(a)]. Accordingly, the other two transitions from -2.0 to 0.7 eV, and from -0.8 to 0.4 eV give the maximum photocurrents at photon energies of 2.7 and 1.2 eV. For the Se1 vacancy defect, by observing Fig. 4(b), the transmission spectrum of the device decreases sharply to 0 in the energy ranges of $-0.7 < E < -0.3$ eV and $1.6 < E < 1.95$ eV. Similarly, there also are several transmission peaks, for example, the peaks at -1.4 , -0.1 , 0.2 , and 0.3 eV. The transition from -0.1 to 0.3 eV induces the largest photocurrent at a photon energy of 0.4 eV. For the Se2 vacancy defect, the transmission is suppressed to zero in the energy range $-0.9 < E < -0.3$ eV due to the effect of the vacancy defect. The transition of electrons between the energies associating with the transmission peaks, for example, the transition from -1.6 to 0.2 eV induces a maximum photocurrent at a photon energy of 1.8 eV. The transmission spectrum can also explain the maximum photocurrent when the linearly polarized light is propagating along the $-y$ axis. The vacancy concentration can slightly affect the zero value of the transmission. For example, when the number of the vacancy decreases from 10 to 6, the zero value of the transmission in the energy range of $-0.9 < E < -0.3$ eV disappears. However, the device with Se vacancy defects can still induce large photocurrents, which can work as an optoelectronic device with excellent functions.

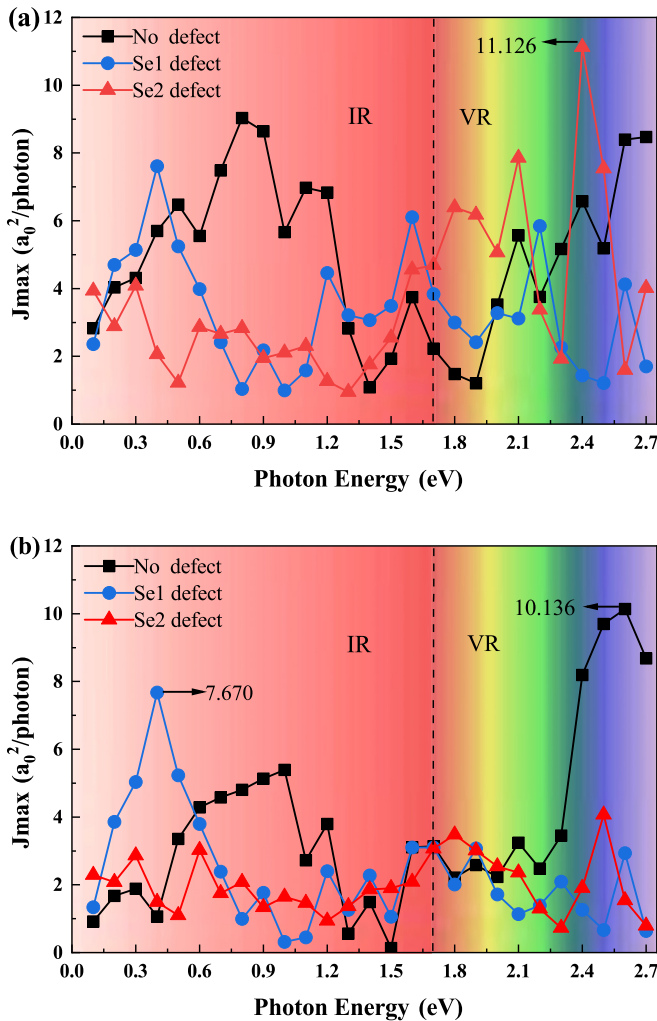


FIG. 3. The maximum photocurrent of the $1T$ - TiSe_2 -based device is plotted as a function of the photon energy for two types of defect configurations. The linearly polarized light propagates along the (a) $-x$ axis and (b) $-y$ axis.

Photodetectors based on two-dimensional materials have excellent performance such as a fast optical response and broadband detection. Sensitivity is an important quality factor to measure the performance of photodetectors. The extinction ratio is generally used to evaluate the sensitivity of devices. Thus we further explore the effect of the vacancy defect on the extinction ratio. The extinction ratio is defined as J_{max}

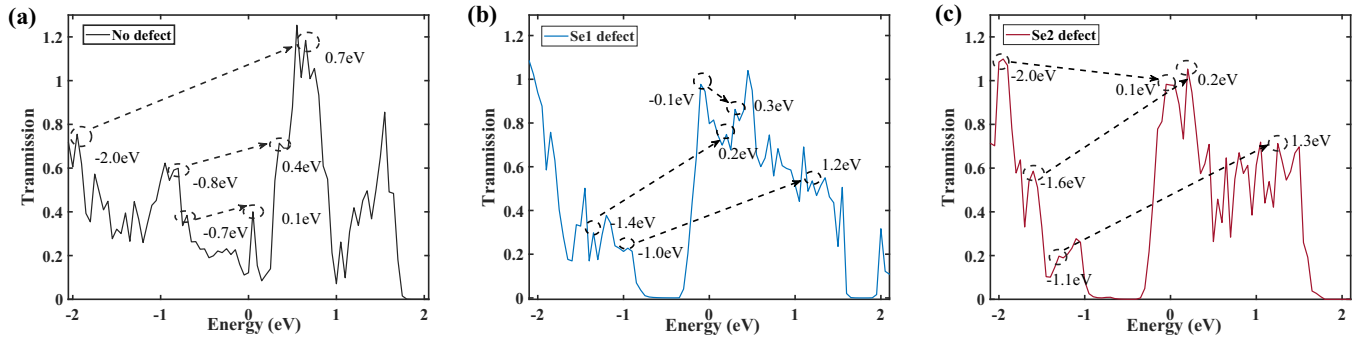


FIG. 4. The transmission is plotted as a function of Fermi energy for two types of defect configurations: (a) no defect, (b) Se1 vacancy defect, (c) Se2 vacancy defect.

over the minimum photocurrent J_{\min} [48,49]. Figure 5(a) shows the extinction ratio of 1T-TiSe₂-based device for two types of defect configurations. With no defect, the extinction ratio has three large peaks, which are 13.06 at a photon energy

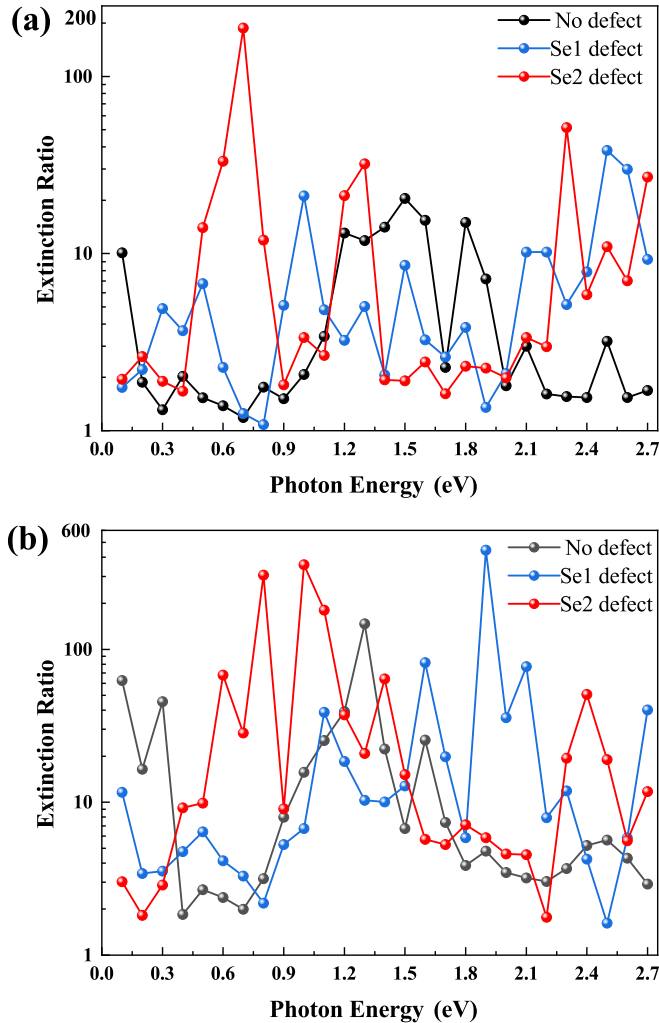


FIG. 5. Extinction ratio of the photocurrent of the 1T-TiSe₂-based device as a function of the photon energy for two types of defect configurations. The linearly polarized light propagates along the (a) $-x$ axis and (b) $-y$ axis.

of 1.2 eV, 20.48 at 1.5 eV, and 14.98 at 1.8 eV. When there exist Se1 vacancy defects (see the blue curve), the largest value of the extinction ratio is about 38.23 at 2.5 eV. Especially, the device with a Se2 vacancy defect can obtain a large extinction ratio with a value of 187.44 at 0.7 eV, which is 157 times that of the device without a defect (1.19 at 0.7 eV). Also, the maximum value of the extinction ratio is much larger than that of black phosphorus-based photodetectors measured in experiments, which is in the range of 1.8–5.8 [50,51]. Figure 5(b) shows the extinction ratio for the linearly polarized light illuminating along the $-y$ axis. With no defect, the extinction ratio has a peak, which is 147.18 at a photon energy of 1.3 eV. When there exist Se1 vacancy defects, the largest value of the extinction ratio is about 445.12 at 1.9 eV. The extinction ratios of the device with a Se2 vacancy defect have two large peaks, namely 306 at 0.8 eV, and 358 at 1.0 eV. It means that the 1T-TiSe₂-based device can significantly improve the extinction ratio, which is a potential candidate for the design of the photodetector. Photoresponsivity is an important figure of merit for a photodetector, which is defined as $R_{\text{ph}} = J_L^{\text{ph}} / (A_S P)$ [52,53], where J_L^{ph} is the real photocurrent, P is the light power density, and A_S is the effective illumination area of the transport channel. When the laser power density is about 0.1–100 W/cm² and A_S is 1 μm^2 , for example, the maximum normalized photocurrent is $J_{\max} = 7.67$ at a photon energy of 0.4 eV for the Se1 defect configuration given in Fig. 3(b). We can calculate the real photocurrent in terms of the formula $J_L^{\text{ph}} = eI_0 J a_0^2 \sqrt{\mu_r / \epsilon_r}$ with $\mu_r = 1$ and $\epsilon_r = 1$ or 10. Then the real photocurrent ranges from 9.65 pA to 30.8 nA, which can be measured experimentally [51,53]. Correspondingly, the photoresponsivity R_{ph} of the TiSe₂ photodetector is about 0.0308 or 0.01 A W⁻¹.

The photoresponsivities of two defect configurations are plotted as a function of the photon energy for the linearly polarized light propagating along the $-x$ and $-y$ axes, as shown in Fig. 6. It can be found that the photoresponsivities show anisotropic behaviors for the two propagating directions. The photoresponsivities of the Se1 and Se2 vacancy defects have relatively large values in the photon energy range of 0–0.6 eV, which can approach to about 0.065 A W⁻¹ for the case of the Se2 defect [see the red triangle curve in Fig. 6(a)]. The photoresponsivities of the case without a defect have relatively large values in the range of 0.6–1.2 eV. The photoresponsivity is the same order as those of monolayer

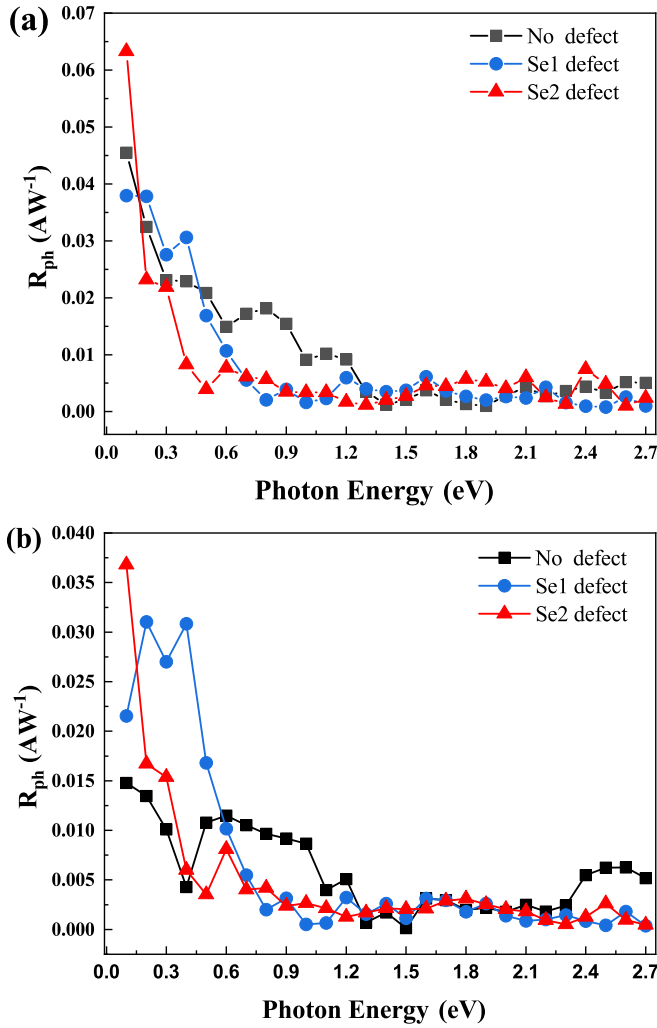


FIG. 6. The photoresponsivities of two types of defect configurations are plotted as a function of the photon energy for the linearly polarized light propagating along the (a) $-x$ axis and (b) $-y$ axis.

MoSi_2P_4 (0.060 A W^{-1}), MoS_2 (0.016 A W^{-1}), monolayer chalcogenides (0.035 A W^{-1} for GeS and 0.075 A W^{-1} for SnS), and monolayer WSe_2 (0.016 A W^{-1}) [54,55]. The disorder induced by the excess atoms can result in a significant decrease of the photocurrent. The spatial photocurrent can demonstrate the exponential decay behavior $J^{\text{ph}}(x) = J_0^{\text{ph}} \exp(-x/L_{\text{ed}})$ with L_{ed} being the effective diffusion length (see Appendix B). The diffusion length can approach to the order of $1\text{--}15 \mu\text{m}$ observed by using the scanning photocurrent microscopy [56,57].

IV. CONCLUSIONS

In summary, we investigate the effect of vacancy defects on the transport properties and the photocurrent of the $\text{Cu-TiSe}_2\text{-Cu}$ heterojunction. The results show that the Se1 and Se2 vacancy defects can induce different photocurrents, which are explained in terms of the transmission spectrum. When the polarized light is illuminated along different directions, the photocurrent gives anisotropic behaviors. The Se vacancy defect can result in a zero value of the transmission, which

can be utilized to modulate the transport property of the TiSe_2 -based device. However, the device with the Se vacancy defects can still induce a large photocurrent, which can work as an optoelectronic device with excellent functions. Especially, the device with the Se2 vacancy defect can induce an extinction ratio with a large value being 157 times that of the device without a defect. The photoresponsivities of a TiSe_2 -based device with vacancy defects can have relatively large values in certain energy ranges. The photocurrent is generated by PGE at zero bias, indicating that the TiSe_2 -based device has the advantage of reducing energy consumption in practical applications. The results can provide important theoretical guidance for the application of $1T\text{-TiSe}_2$ in the field of optoelectronics.

ACKNOWLEDGMENTS

We would like to thank Dr. F.-H. Jia and R.-X. Li for helpful discussions. This work was supported by National Key R&D Program of China under Grants No. 2021YFA1400900, No. 2021YFA0718300, and No. 2021YFA1402100, NSFC under Grants No. 61835013, No. 11574067, No. 12174461, and No. 12234012, Space Application System of China Manned Space Program, and the Natural Science Foundation of Zhejiang Province (Grant No. LTGS24E060005).

APPENDIX A: DERIVATION OF THE PHOTOCURRENT

In this paper, we focus on the modulation of photocurrent of the $1T\text{-TiSe}_2$ heterojunction. The electromagnetic potential is regarded as a weak interaction, and we can discard the nonlinear term in the vector potential. Thus the Hamiltonian can be written as

$$\hat{H} = \frac{\hat{p}^2}{2m_0} + U + \frac{e}{m_0} \hat{A} \cdot \hat{p}, \quad (\text{A1})$$

with $\hat{H}_1 = \frac{e}{m_0} \vec{A} \cdot \hat{p}$. When single-mode monochromatic light is taken into account, \vec{A} can be written as

$$\vec{A}(x, t) = \vec{A}_0(x) (\hat{d}^\dagger e^{i\omega t} + \hat{d} e^{-i\omega t}), \quad (\text{A2})$$

where \hat{d}^\dagger and \hat{d} are the bosonic creation and annihilation operators. $\vec{A}_0(x)$ can be obtained by solving the equation $\nabla^2 \vec{A}_0(x) + \frac{\omega^2}{c^2} \vec{A}_0(x) = 0$. Assuming an isotropic, homogeneous susceptibility, and dielectric coefficient, the vector potential \vec{A} is given by

$$\vec{A}(x, t) = \vec{e} \left(\frac{\hbar I_0 \sqrt{\mu_r \epsilon_r}}{2N\omega\epsilon c} \right)^{1/2} (\hat{d}^\dagger e^{i\omega t} + \hat{d} e^{-i\omega t}), \quad (\text{A3})$$

where \vec{e} is the polarization direction of the field. Utilizing the site basis, the second-quantized form of the perturbation Hamiltonian is given by $\hat{H}_1 = \sum_{m,n} \langle m | \hat{H}_1 | n \rangle \hat{c}_m^\dagger \hat{c}_n$, where $|m\rangle$ and $|n\rangle$ are site-basis states with m and n designating sites in real space. Thus the matrix element is

$$\hat{H}_{mn}^1 = \langle m | \hat{H}_1 | n \rangle = \frac{e}{m_0} \vec{A} \cdot \langle m | \hat{p} | n \rangle. \quad (\text{A4})$$

Accordingly, the perturbation Hamiltonian is given by

$$\hat{H}_1 = \sum_{mn} \xi_{mn} (\hat{d}^\dagger e^{i\omega t} + \hat{d} e^{-i\omega t}) \hat{c}_m^\dagger \hat{c}_n, \quad (\text{A5})$$

where ξ_{mn} is defined as

$$\xi_{mn} = \frac{e}{m_0} \left(\frac{\hbar I_\omega \sqrt{u_r \varepsilon_r}}{2N\omega \varepsilon C} \right)^{\frac{1}{2}} \hat{e} \cdot \langle m | \hat{p} | n \rangle. \quad (\text{A6})$$

$J_L^{(\text{ph})}$ is proportional to the density of number of photons (N/V) or photon flux I_ω , which can be calculated in terms of the equation

$$J_L^{(\text{ph})} = \frac{ie}{h} \int \text{Tr} \{ \Gamma_L [G^{<(\text{ph})} + f_L(G^{>(\text{ph})} - G^{<(\text{ph})})] \} dE. \quad (\text{A7})$$

Thus one can obtain the photocurrent response function $J = J_L^{(\text{ph})}/(eI_\omega)$. In terms of the coupled-field theory [43], the lowest-order contribution of self-energies in the site basis for photon-electron interactions is given by

$$\Sigma_{mn}^{>/<(\text{ph})}(t_1, t_2) = \sum_{ij} G_{0,ij}^{>/<}(t_1, t_2) \mathbb{R}_{mi,jn}^{>/<}(t_1, t_2), \quad (\text{A8})$$

where $G_0^{>/<}$ refer to the lesser/greater Green's functions without the photon-electron interactions. The photon propagators $\mathbb{R}^{>/<}$ can be written as

$$\begin{aligned} \mathbb{R}_{mi,jn}^{<}(t_1, t_2) &= \langle \hat{H}_{jn}^1(t_2) \hat{H}_{mi}^1(t_1) \rangle, \\ \mathbb{R}_{mi,jn}^{>}(t_1, t_2) &= \langle \hat{H}_{mi}^1(t_1) \hat{H}_{jn}^1(t_2) \rangle, \end{aligned} \quad (\text{A9})$$

where the bosonic operators satisfy the following relations,

$$\begin{aligned} \langle \hat{d}^\dagger(t_1) \hat{d}(t_2) \rangle &= N e^{i\omega(t_1-t_2)}, \\ \langle \hat{d}(t_1) \hat{d}^\dagger(t_2) \rangle &= (N+1) e^{-i\omega(t_1-t_2)}, \\ \langle \hat{d}(t_1) \hat{d}(t_2) \rangle &= \langle \hat{d}^\dagger(t_1) \hat{d}^\dagger(t_2) \rangle = 0. \end{aligned} \quad (\text{A10})$$

Then we have

$$\begin{aligned} \mathbb{R}_{mi,jn}^{<} &= 2\pi \xi_{mi} \xi_{jn} [N \delta(E - \hbar\omega) \\ &\quad + (N+1) \delta(E + \hbar\omega)], \\ \mathbb{R}_{mi,jn}^{>} &= 2\pi \xi_{mi} \xi_{jn} [N \delta(E + \hbar\omega) \\ &\quad + (N+1) \delta(E - \hbar\omega)]. \end{aligned} \quad (\text{A11})$$

Accordingly, one can obtain the self-energies

$$\begin{aligned} \Sigma_{mn}^{<(\text{ph})}(E) &= \sum_{ij} \xi_{mi} \xi_{jn} [N G_{0,ij}^{<}(E - \hbar\omega) \\ &\quad + (N+1) G_{0,ij}^{<}(E + \hbar\omega)], \\ \Sigma_{mn}^{>(\text{ph})}(E) &= \sum_{ij} \xi_{mi} \xi_{jn} [N G_{0,ij}^{>}(E + \hbar\omega) \\ &\quad + (N+1) G_{0,ij}^{>}(E - \hbar\omega)]. \end{aligned} \quad (\text{A12})$$

The matrix forms of the self-energies including the photon-electron interaction are given by

$$\begin{aligned} \Sigma^{<(\text{ph})}(E) &= N \xi \mathbf{G}_0^{<}(E - \hbar\omega) \xi^\dagger \\ &\quad + (N+1) \xi^\dagger \mathbf{G}_0^{<}(E + \hbar\omega) \xi, \\ \Sigma^{>(\text{ph})}(E) &= N \xi^\dagger \mathbf{G}_0^{>}(E + \hbar\omega) \xi \\ &\quad + (N+1) \xi \mathbf{G}_0^{>}(E - \hbar\omega) \xi^\dagger. \end{aligned} \quad (\text{A13})$$

The greater/lesser Green's function $G^{>/<(\text{ph})}$ including the photon-electron interaction can be written as

$$G^{>/<(\text{ph})}(E) = G_0^R(E) \Sigma^{>/<(\text{ph})}(E) G_0^A(E), \quad (\text{A14})$$

where $G_0^{R/A}$ refers to the retarded/advanced Green's function without the photon-electron interaction. Correspondingly,

$$\begin{aligned} \mathbf{G}^{<(\text{ph})}(E) &= \mathbf{G}_0^R (N \xi \mathbf{G}_0^{<}(E - \hbar\omega) \xi^\dagger \\ &\quad + (N+1) \xi^\dagger \mathbf{G}_0^{<}(E + \hbar\omega) \xi) \mathbf{G}_0^A, \\ \mathbf{G}^{>(\text{ph})}(E) &= \mathbf{G}_0^R (N \xi^\dagger \mathbf{G}_0^{>}(E + \hbar\omega) \xi \\ &\quad + (N+1) \xi \mathbf{G}_0^{>}(E - \hbar\omega) \xi^\dagger) \mathbf{G}_0^A, \end{aligned} \quad (\text{A15})$$

where the first term arises from the contribution of the excitation of an electron by the absorption of a photon and the second term corresponds to the emission of a photon by deexcitation of an electron. In this paper, it is assumed that absorption processes completely dominate, thus the emission terms, namely the second term in the lesser and greater Green's functions, can be neglected. For the linearly polarized light, the polarized vector is $\hat{e} = \cos \theta \hat{e}_1 + \sin \theta \hat{e}_2$. In terms of Eq. (A6), one can obtain $\xi = C_0^{1/2} \hat{e} \cdot \vec{p}$. Substituting ξ into Eq. (A15), we have

$$\begin{aligned} G^{<(\text{ph})}(E) &= G_0^R C_0 \left(\cos^2 \theta \sum_{\alpha\beta} e_{1\alpha} p_\alpha^\dagger N G_0^{<}(E - \hbar\omega) e_{1\beta} p_\beta + \sin^2 \theta \sum_{\alpha\beta} e_{2\alpha} p_\alpha^\dagger N G_0^{<}(E - \hbar\omega) e_{2\beta} p_\beta \right. \\ &\quad \left. + \frac{\sin 2\theta}{2} \sum_{\alpha\beta} e_{1\alpha} p_\alpha^\dagger N G_0^{>}(E - \hbar\omega) e_{2\beta} p_\beta + \frac{\sin 2\theta}{2} \sum_{\alpha\beta} e_{2\alpha} p_\alpha^\dagger N G_0^{<}(E - \hbar\omega) e_{1\alpha} p_\alpha \right) G_0^A, \\ G^{>(\text{ph})}(E) &= G_0^R C_0 \left(\cos^2 \theta \sum_{\alpha\beta} e_{1\alpha} p_\alpha^\dagger N G_0^{>}(E + \hbar\omega) e_{1\beta} p_\beta + \sin^2 \theta \sum_{\alpha\beta} e_{2\alpha} p_\alpha^\dagger N G_0^{>}(E + \hbar\omega) e_{2\beta} p_\beta \right. \\ &\quad \left. + \frac{\sin 2\theta}{2} \sum_{\alpha\beta} e_{1\alpha} p_\alpha^\dagger N G_0^{>}(E + \hbar\omega) e_{2\beta} p_\beta + \frac{\sin 2\theta}{2} \sum_{\alpha\beta} e_{2\alpha} p_\alpha^\dagger N G_0^{>}(E + \hbar\omega) e_{1\alpha} p_\alpha \right) G_0^A. \end{aligned} \quad (\text{A16})$$

Then we can obtain the formula of the photocurrent given in Eq. (1).

APPENDIX B: THE DRIFT-DIFFUSION FORMALISM FOR THE PHOTOCURRENT

To extract the diffusion length of the photogenerated carrier from the scanning photocurrent microscopy, one can obtain the dependent relation of the diffusion length on the decay behavior of the observed photocurrent in the real space. The drift-diffusion equation for a single type of excess carrier δn in the simplified case of one-dimensional transport can be written as

$$\frac{\partial \delta n}{\partial t} = \mathbb{D} \frac{\partial^2 \delta n}{\partial x^2} + \mu \mathbb{E} \frac{\partial \delta n}{\partial x} + \mathbb{G} - \frac{\delta n}{\tau}, \quad (\text{B1})$$

where \mathbb{D} is the diffusion coefficient of the carriers, \mathbb{G} is the generation rate, μ is the mobility, \mathbb{E} is the amplitude of the electric field, and τ is the carrier lifetime. For the steady state illumination ($d\delta n/dt = 0$) with a negligibly small electric field, the diffusion equation evolves to

$$\mathbb{D} \frac{\partial^2 \delta n}{\partial x^2} = \frac{\delta n}{\tau}. \quad (\text{B2})$$

By solving the above equation, we can obtain

$$\delta n = \delta n_0 \exp\left(-\frac{x}{L_d}\right), \quad (\text{B3})$$

where $x(> 0)$ is the distance between the collection electrode and the generation point, δn_0 is the excess photogenerated carrier of the generation point, and L_d is the diffusion length with $L_d = \sqrt{\mathbb{D}\tau}$. By considering the diffusion behavior, the spatial photocurrent can be written as

$$J^{\text{ph}}(x) = -\mathbb{D} \frac{\partial \delta n}{\partial x}. \quad (\text{B4})$$

Since the diffusion length L_d depends on $\delta n(x)$, the photocurrent can be changed to

$$J^{\text{ph}}(x) = J_0^{\text{ph}} \exp\left(-\frac{x}{L_{\text{ed}}}\right), \quad (\text{B5})$$

where L_{ed} is the effective diffusion length. In MAPbBr₃ single crystals, the effective diffusion length of electrons and holes can approach to the order of 1–15 μm [56,57]. Correspondingly, in the 1T-TiSe₂ heterojunction, it is expected that the spatial photocurrent will also give the exponential decay behavior. It is deserved to analyze the effective diffusion length in the subsequent investigation.

-
- [1] A. K. Geim and K. S. Novoselov, *Nat. Mater.* **6**, 183 (2007).
- [2] Y. P. An, Y. S. Hou, K. Wang, S. J. Gong, C. L. Ma, C. X. Zhao, T. X. Wang, Z. Y. Jiao, H. Y. Wang, and R. Q. Wu, *Adv. Funct. Mater.* **30**, 2002939 (2020).
- [3] V. Podzorov, M. E. Gereshenson, C. Kloc, R. Zeis, and E. Bucher, *Appl. Phys. Lett.* **84**, 3301 (2004).
- [4] S. Kim, A. Konar, W. S. Hwang, J. H. Lee, J. Lee, J. Yang, C. Jung, H. Kim, J. B. Yoo, J. Y. Choi, Y. W. Jin, S. Y. Lee, D. Jena, W. Choi, and K. Kim, *Nat. Commun.* **3**, 1011 (2012).
- [5] D. H. Keum, S. Cho, J. H. Kim, D. H. Choe, H. J. Sung, M. Kan, H. Kang, J. Y. Hwang, S. W. Kim, H. Yang, K. J. Chang, and Y. H. Lee, *Nat. Phys.* **11**, 482 (2015).
- [6] L. L. Hu, F. Sun, H. Zhao, and J. M. Zhao, *Opt. Lett.* **44**, 5214 (2019).
- [7] W. X. Zhang, Z. S. Huang, and W. L. Zhang, *Nano Res.* **7**, 1731 (2014).
- [8] Q. H. Wang, K. K. Zadeh, A. Kis, J. N. Coleman, and M. S. Strano, *Nat. Nanotechnol.* **7**, 699 (2012).
- [9] Z. Ben Aziza, D. Pierucci, H. Henck, M. G. Silly, C. David, M. Yoon, F. Sirotti, K. Xiao, M. Eddrief, J. C. Girard, and A. Ouerghi, *Phys. Rev. B* **96**, 035407 (2017).
- [10] K. F. Mak, C. Lee, J. Hone, J. Shan, and T. F. Heinz, *Phys. Rev. Lett.* **105**, 136805 (2010).
- [11] C. Ruppert, O. B. Aslan, and T. F. Heinz, *Nano Lett.* **14**, 6231 (2014).
- [12] S. Tongay, J. Zhou, C. Ataca, K. Lo, T. S. Matthews, J. B. Li, J. C. Grossman, and J. Wu, *Nano Lett.* **12**, 5576 (2012).
- [13] R. Wu, Y. L. Zhang, S. C. Yan, F. Bian, W. L. Wang, X. D. Bai, X. H. Lu, J. M. Zhao, and E. G. Wang, *Nano Lett.* **11**, 5159 (2011).
- [14] Y. L. Wu, Q. Wu, F. Sun, C. Cheng, S. Meng, and J. M. Zhao, *Proc. Natl. Acad. Sci. USA* **112**, 11800 (2015).
- [15] W. H. Wang, Y. L. Wu, Q. Wu, J. J. Hua, and J. M. Zhao, *Sci. Rep.* **6**, 22072 (2016).
- [16] D. Wickramaratne, S. Subedi, D. H. Torchinsky, G. Karapetrov, and I. I. Mazin, *Phys. Rev. B* **105**, 054102 (2022).
- [17] K. Sugawara, Y. Nakata, R. Shimizu, P. Han, T. Hitosugi, T. Sato, and T. Takahashi, *ACS Nano* **10**, 1341 (2016).
- [18] M. H. Liao, H. Wang, Y. Y. Zhu, R. Shang, M. Rafique, L. X. Yang, H. Zhang, D. Zhang, and Q. K. Xue, *Nat. Commun.* **12**, 5342 (2021).
- [19] E. Morosan, H. W. Zandbergen, B. S. Dennis, J. W. G. Bos, Y. Onose, T. Klimczuk, A. P. Ramirez, N. P. Ong, and R. J. Cava, *Nat. Phys.* **2**, 544 (2006).
- [20] A. N. Titov, V. L. Konstantinov, V. N. Neverov, E. A. Neifeld, and L. S. Krasavin, *J. Supercond. Novel Magn.* **19**, 73 (2006).
- [21] F. J. Di Salvo, D. E. Moncton, and J. V. Waszczak, *Phys. Rev. B* **14**, 4321 (1976).
- [22] M. J. Wei, W. J. Lu, R. C. Xiao, H. Y. Lv, P. Tong, W. H. Song, and Y. P. Sun, *Phys. Rev. B* **96**, 165404 (2017).
- [23] P. Li, X. B. Zheng, H. X. Yu, G. Q. Zhao, J. Shu, X. Xu, W. P. Sun, and S. X. Dou, *Energy Storage Mater.* **16**, 512 (2019).
- [24] B. Z. Yan, B. T. Zhang, H. K. Nie, G. R. Li, X. L. Sun, Y. R. Wang, J. T. Liu, B. N. Shi, S. D. Liu, and J. L. He, *Nanoscale* **10**, 20171 (2018).
- [25] G. L. Li, W. H. Du, S. Sun, Q. M. Lu, Z. X. Chen, H. L. Liu, Y. D. Ma, X. L. Sun, Y. C. Jia, and F. Chen, *Nanophotonics* **11**, 3383 (2022).
- [26] R. F. Wei, X. L. Tian, L. P. Yang, D. D. Yang, Z. J. Ma, H. Guo, and J. R. Qiu, *Nanoscale* **11**, 22277 (2019).
- [27] G. Rohde, T. Rohwer, A. Stange, C. Sohr, K. Hanff, L. X. Yang, L. Kipp, K. Rossnagel, and M. Bauer, *J. Electron Spectrosc.* **5**, 46295 (2014).

- [28] J. Hasaien, K. J. Zhu, F. Sun, Y. L. Wu, Y. G. Shi, and J. M. Zhao, *Acta Phys. Sin.* **69**, 207801 (2020).
- [29] X. L. Zhang, L. F. Liu, and W. M. Liu, *Sci. Rep.* **3**, 2908 (2013).
- [30] U. P. Sahoo, S. Anupam, B. Das, M. K. Sikdar, L. Nanda, and P. K. Sahoo, *ACS Appl. Nano Mater.* **5**, 4072 (2022).
- [31] U. P. Sahoo, A. Mukherejee, and P. K. Sahoo, *ACS Appl. Nano Mater.* **40**, 665 (2022).
- [32] Z. P. Song, J. X. Yi, J. Qi, Q. Zheng, Z. L. Zhu, L. Tao, Y. Cao, Y. Li, Z. Y. Gao, R. Z. Zhang, L. Huang, G. Li, Z. Q. Xu, X. Wu, Y. L. Wang, C. M. Shen, Y. Y. Zhang, H. L. Lu, X. Lin, S. X. Du *et al.*, *Nano Res.* **15**, 4687 (2022).
- [33] X. R. Wang, Y. Ding, M. N. Chen, Z. B. Siu, M. B. A. Jalil, and Y. Li, *Opt. Lett.* **47**, 906 (2022).
- [34] Y. Ding, X. R. Wang, L. H. Liao, X. Y. Cheng, J. Y. Zhang, Y. Y. Wang, H. Ying, and Y. Li, *Opt. Lett.* **47**, 4881 (2022).
- [35] Y. Gao, Y. Zhang, and D. Xiao, *Phys. Rev. Lett.* **124**, 077401 (2020).
- [36] J. Chen, L. W. Zhang, L. Zhang, X. H. Zheng, L. Xiao, S. Jia, and J. Wang, *Phys. Chem. Chem. Phys.* **20**, 26744 (2018).
- [37] Y. Peng, X. T. Liu, Z. H. Sun, C. M. Ji, L. N. Li, Z. Y. Wu, S. S. Wang, Y. P. Yao, M. C. Hong, and J. H. Luo, *Angew. Chem., Int. Ed.* **59**, 3933 (2020).
- [38] O. Matsyshyn, F. Piazza, R. Moessner, and I. Sodemann, *Phys. Rev. Lett.* **127**, 126604 (2021).
- [39] T. Morimoto and N. Nagaosa, *Sci. Adv.* **2**, e1501524 (2016).
- [40] C. M. Fang, R. A. de Groot, and C. Haas, *Phys. Rev. B* **56**, 4455 (1997).
- [41] Y. Q. Xie, M. Y. Chen, Z. W. Wu, Y. B. Hu, Y. Wang, J. Wang, and H. Guo, *Phys. Rev. Appl.* **10**, 034005 (2018).
- [42] J. P. Perdew, K. Burke, and M. Ernzerhof, *Phys. Rev. Lett.* **77**, 3865 (1996).
- [43] L. E. Henrickson, *J. Appl. Phys.* **91**, 6273 (2002).
- [44] Y. Q. Xie, L. Zhang, Y. Zhu, L. Liu, and H. Guo, *Nanotechnology* **26**, 455202 (2015).
- [45] M. P. L. Sancho, J. M. L. Sancho, and J. J. Rubio, *J. Phys. F: Met. Phys.* **15**, 851 (1985).
- [46] J. Hu, W. Xiong, C. Z. Cai, J. W. Wang, J. J. Li, Y. Q. Xie, and Y. Wang, *Appl. Phys. Lett.* **115**, 151104 (2019).
- [47] V. I. Belinicher and B. I. Sturman, *Sov. Phys. Usp.* **23**, 199 (1980).
- [48] Z. H. Xu, Z. Chen, and Q. M. Yuan, *Phys. E* **133**, 114846 (2021).
- [49] F. H. Chu, M. Y. Chen, Y. Wang, Y. Q. Xie, B. Y. Liu, Y. H. Yang, X. T. An, and Y. Z. Zhang, *J. Mater. Chem. C* **6**, 2509 (2018).
- [50] H. T. Yuan, X. G. Liu, F. Afshinmanesh, W. Li, G. Xu, J. Sun, B. Lian, A. G. Curto, G. J. Ye, Y. Hikita, Zh. X. Sh, Sh. Ch. Zhang, X. H. Chen, M. Brongersma, H. Y. Hwang, and Y. Cui, *Nat. Nanotechnol.* **10**, 707 (2015).
- [51] T. Hong, B. Chamlagain, W. Lin, H. J. Chuang, M. H. Pan, Zh. X. Zhou, and Y. Q. Xu, *Nanoscale* **6**, 8978 (2014).
- [52] M. W. Yu, Y. T. Lin, Ch. H. Wu, T. J. Wang, J. H. Cyue, J. Kikkawa, S. Ishii, T. Ch. Lu, K. P. Chen, *Appl. Surf. Sci.* **642**, 158541 (2024).
- [53] J. Wu, G. K. W. Koon, D. Xiang, C. Han, C. T. Toh, E. S. Kulkarni, I. Verzhbitskiy, A. Carvalho, A. S. Rodin, S. P. Koenig, G. Eda, W. Chen, A. H. Castro Neto, and B. Ozyilmaz, *ACS Nano* **9**, 8070 (2015).
- [54] A. Pospischil, M. M. Furchi, and T. Mueller, *Nat. Nanotechnol.* **9**, 257 (2014).
- [55] H. Yao, C. Zhan, Q. Wang, J. W. Li, Y. J. Yu, F. M. Xu, B. Wang, and Y. D. Wei, *Nanomaterials* **11**, 559 (2021).
- [56] N. Ganesh, A. Ghorai, S. Krishnamurthy, S. Banerjee, K. L. Narasimhan, S. B. Ogale, and K. S. Narayan, *Phys. Rev. Mater.* **4**, 084602 (2020).
- [57] T. Otto, C. Miller, J. Tolentino, Y. Liu, M. Law, and D. Yu, *Nano Lett.* **13**, 3463 (2013).